TÜBİTAK

Turkish Journal of Chemistry

http://journals.tubitak.gov.tr/chem/

Research Article

Turk J Chem
(2018) 42: 448 – 459

doi:10.3906/kim-1707-69

Application of the Taguchi approach to optimize ZnO synthesis via hydrothermally assisted sol-gel method

Zahra KHAGHANPOUR, Sanaz NAGHIBI*
Department of Technical and Engineering, Shahreza Branch, Islamic Azad University, Shahreza, Iran

Received: 25.07.2017 • **Accepted/Published Online:** 24.11.2017 • **Final Version:** 27.04.2018

Abstract: ZnO powder was synthesized via a hydrothermally assisted sol-gel method. Synthesis variables including Zn-precursor type, pH value, time, and temperature of hydrothermal treatment were analyzed using the Taguchi approach. The experimental procedures were defined based on the L9 array for four variables in three levels. The influences of those variables on the response parameters, i.e. crystallite size, crystallinity, band gap energy (E_g), and degradation constants (k), were evaluated. XRD results and E_g values showed that ZnO wurtzite appeared to be the only crystalline phase in the samples. Taguchi analysis predicted that the optimized conditions to achieve the highest photoactivity are as follows: Zn-precursor = zinc acetate, pH = 8, t = 2 h, and T = 150 °C. The optimized sample was synthesized based on the mentioned conditions and characterized. The obtained results confirmed the prediction of the Taguchi method and the highest k value was observed.

Key words: ZnO, hydrothermally assisted sol-gel method, Taguchi approach, photoactivity

1. Introduction

Zinc oxide, as a well-known semiconductor ceramic, has been investigated in detail. Preparation methods,[1–6] morphologies,[7–9] applications,[10–13] and modification processes[14–16] of ZnO are topics of high current interest. The photocatalytic performance of this material is very important[17–19] in various fields of applications such as solar cells,[20,21] water treatment,[22,23] medicine,[24–26] etc.

The improvement in photocatalytic performance of ZnO has been investigated by adjusting preparation conditions,[27,28] morphology,[7] particle size,[29] dopant agent,[15,16] and crystallinity.[30] Previous studies have shown that the photocatalytic activity of a photocatalyst is seriously dependent on decreasing the particle size and increasing the degree of crystallinity. The hydrothermally assisted sol-gel technique is an appropriate method to control these parameters.[31] The effect of parameters on the characteristics of the as-synthesized specimens has been previously investigated.[32–34] However, these studies have used direct methods and therefore only a limited number of parameters could be evaluated. The statistical methods are based on the optimization of a procedure without the requirement to survey a large number of parameters. The Taguchi statistical method is one of the powerful and well-known techniques used to facilitate the study of materials chemistry.[31,35–38]

In this research, the Taguchi approach was utilized to design an experimental procedure for ZnO synthesis via the hydrothermally assisted sol-gel method. The precursor type, pH value of the sol, and temperature and time of the hydrothermal treatment were chosen as the variables. The degree of crystallinity, the average

*Correspondence: naghibi@iaush.ac.ir

crystallite size, and the *Eg* value were calculated as the intermediate responses. The degradation constant (k) as an index of the photoactivity was defined as the response parameter. The Taguchi L9 array was chosen to investigate four variables in three levels. The variables were analyzed and the optimized conditions were determined and utilized to prepare a sample. The characteristics of the optimized sample were also examined.

2. Results and discussion

2.1. Characterization results

Figure 1 shows the XRD patterns of the as-prepared powder samples. All of them consisted of ZnO with PDF No. 75-576 and no crystalline impurity could be observed. The difference between the XRD patterns arises essentially from the intensity of the peaks and consequently crystallinity and crystallite size would be different. These parameters were calculated and are provided in Table 1.

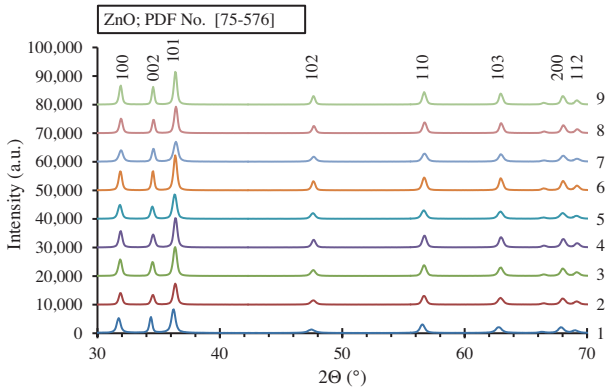

Figure 1. XRD patterns of the as-synthesized samples. The circles refer to the standard peak positions of ZnO wurtzite crystal structure [PDF No. 75-576].

Table 1. Numerical parameters related to the samples, including height of peak, average crystallite size, degree of crystallinity, band gap energy, and apparent rate constants of MB degradation.

Sample code	XRD			DRS	UV-Vis
	Height of peak at ~36°	Average crystallite size (nm)	Degree of crystallinity (%)	E_g (eV)	K (min^{-1})
1	8361	35	69	3.25	0.0109
2	7367	20	85	3.22	0.0132
3	10163	35	84	3.23	0.0129
4	10262	15	86	3.22	0.0178
5	8549	32	82	3.22	0.0176
6	12259	22	86	3.24	0.0156
7	6999	35	80	3.29	0.0100
8	9287	46	88	3.25	0.0125
9	11476	69	86	3.24	0.0092

Figure 2 shows the Tauc curves calculated from the DRS results. The *Eg* values of the samples were obtained from these curves and are provided in Table 1. As can be seen, these values are very close and range from 3.22 to 3.29 eV.

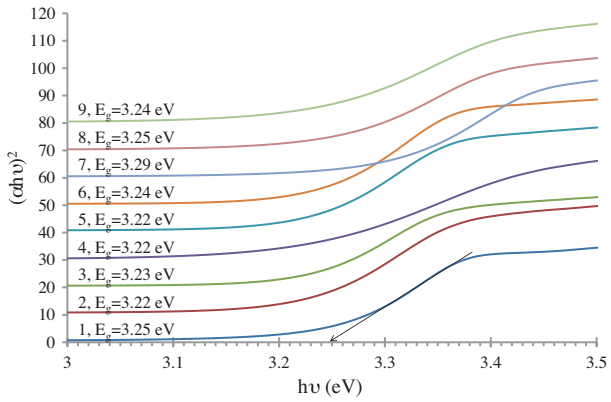

Figure 2. Tauc plots of the as-synthesized samples.

The photocatalytic performance of the samples was evaluated by degradation of methylene blue in aqueous solution under direct UV irradiation. Figure 3 shows the 'ln (C_0/C)' vs. 'UV irradiation time'. The degradation constants (k) of the samples are equal to the intercept of trend lines. These values were calculated and are provided in Table 1.

2.2. Taguchi analysis of the numerical results

Based on the available numerical data in Table 1 and according to the Taguchi method, Figures 4A–4D were drawn, illustrating the effects of the mentioned parameters on the average crystallite size, degree of crystallinity, band gap energy, and apparent rate constants of MB degradation (k), respectively. On the other hand, the influence percentage and ranking of the factors on the evaluated parameters were calculated by Minitab software and are provided in Table 2.

Table 2. Influence percentage and ranking of the factors on the evaluated parameters.

Factors	Zn-precursor		Temperature		Time		pH	
Indexes	%	Rank	%	Rank	%	Rank	%	Rank
Average crystallite size	44	1	23	3	1	4	32	2
Degree of crystallinity	22	3	29	2	20	4	29	1
E_g	35	1	25	2	22	3	18	4
k	55	1	14	4	16	2	15	3

2.2.1. Crystallite size

The crystallite size is indicative of a series of atoms having the same orientation in one crystal. It is known as the dimension of a coherently diffracting domain in the crystalline structure. This is dependent on the formation of point defects and dislocations in the as-synthesized crystals.[39] Therefore, variation in the average crystallite size is an important variable affecting the physical as well as photocatalytic properties.

Figure 4A shows that Zn-precursor type and pH value have the largest effect on the average crystallite size. It is clear that zinc chloride is responsible for the largest crystallite size. To investigate this issue, TEM images of three selected samples, i.e. sample 2 (containing zinc nitrate), sample 4 (containing zinc acetate), and sample 9 (containing zinc chloride), were taken and are shown in Figures 5A–5F. These images confirmed

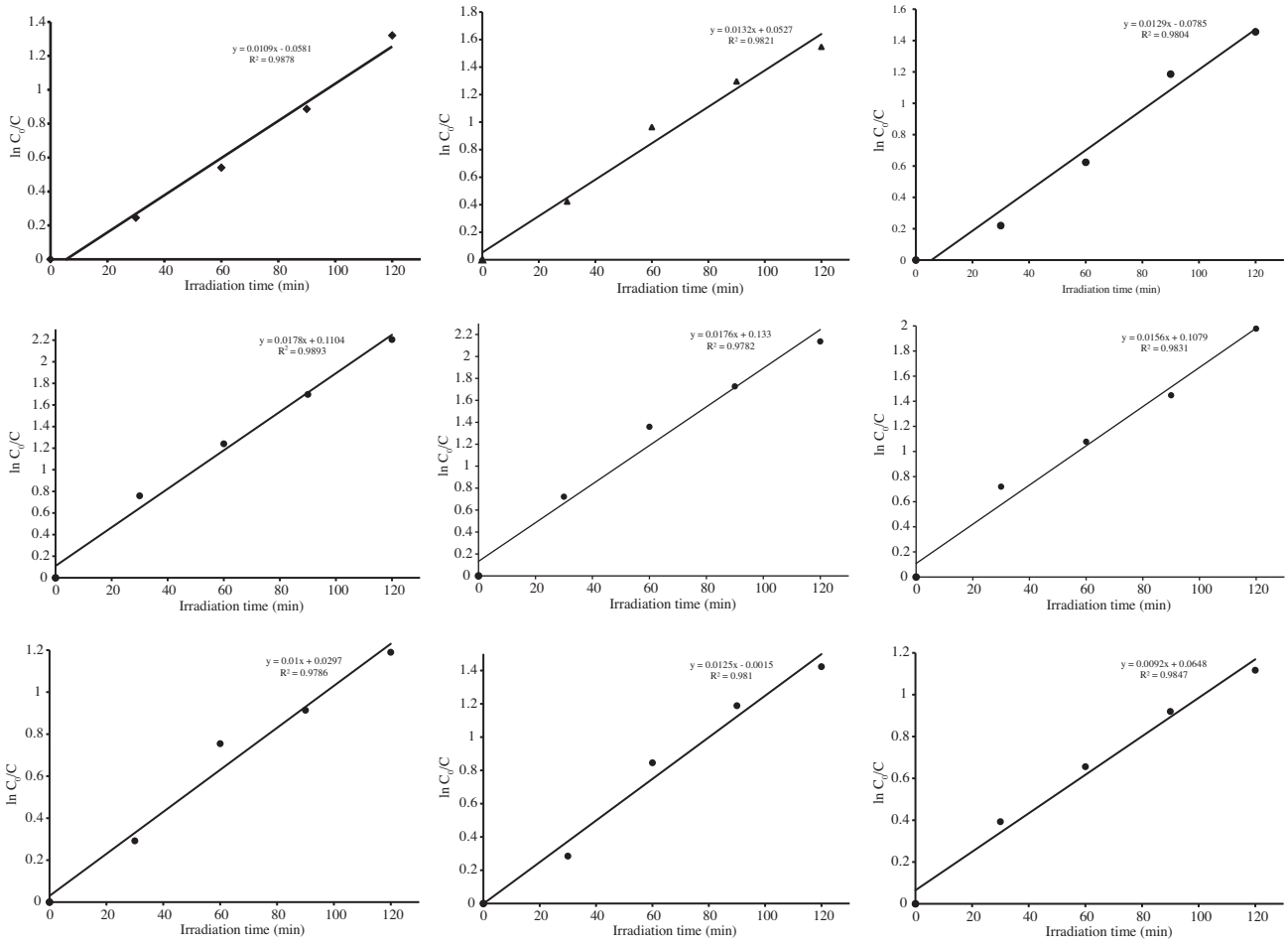

Figure 3. Kinetics of the photodegradation of MB solution containing the as-synthesized powder samples. The first-order kinetics are consistent with the lines due to the high values of R^2.

the crystallite size results. Sample 2 contains semispherical particles with particle size distribution of 50–100 nm. Sample 4 consists of rod-like particles with a length of ˜100 nm and a diameter of ˜30 nm. Unlike the two previous samples, the microstructure of sample 9 was changed. The particles grew extensively and micron-sized hexagonal flakes were formed. The exaggerated growth of the particles from the zinc chloride precursor is responsible for the larger crystallite size in this series of samples. Pourrahimi et al. studied the effect of zinc salt on the grain size of ZnO particles. They stated that, during ZnO crystallization, some petals are formed from an oriented self-assembly and condensation of the nanoprisms. Then octahedrons are shaped from the petals and interconnect to shape polygons. The polygons consequently grow into larger particles in the chloride case by migration and addition of crystallites via dissolution and reprecipitation. The other Zn salts (nitrate and acetate) have a strong ability to prolong the stabilization of the as-formed crystallites.[40] Even though the mechanism of ZnO formation is beyond the aim of the present research, it should be mentioned that this subject has been investigated thoroughly.[9,41–43]

The pH value is another parameter that has a considerable influence on the crystallite size. By increasing the pH value from 8 to 9, crystallite size increased, whereas more increase in pH up to 10 led to the decrease of

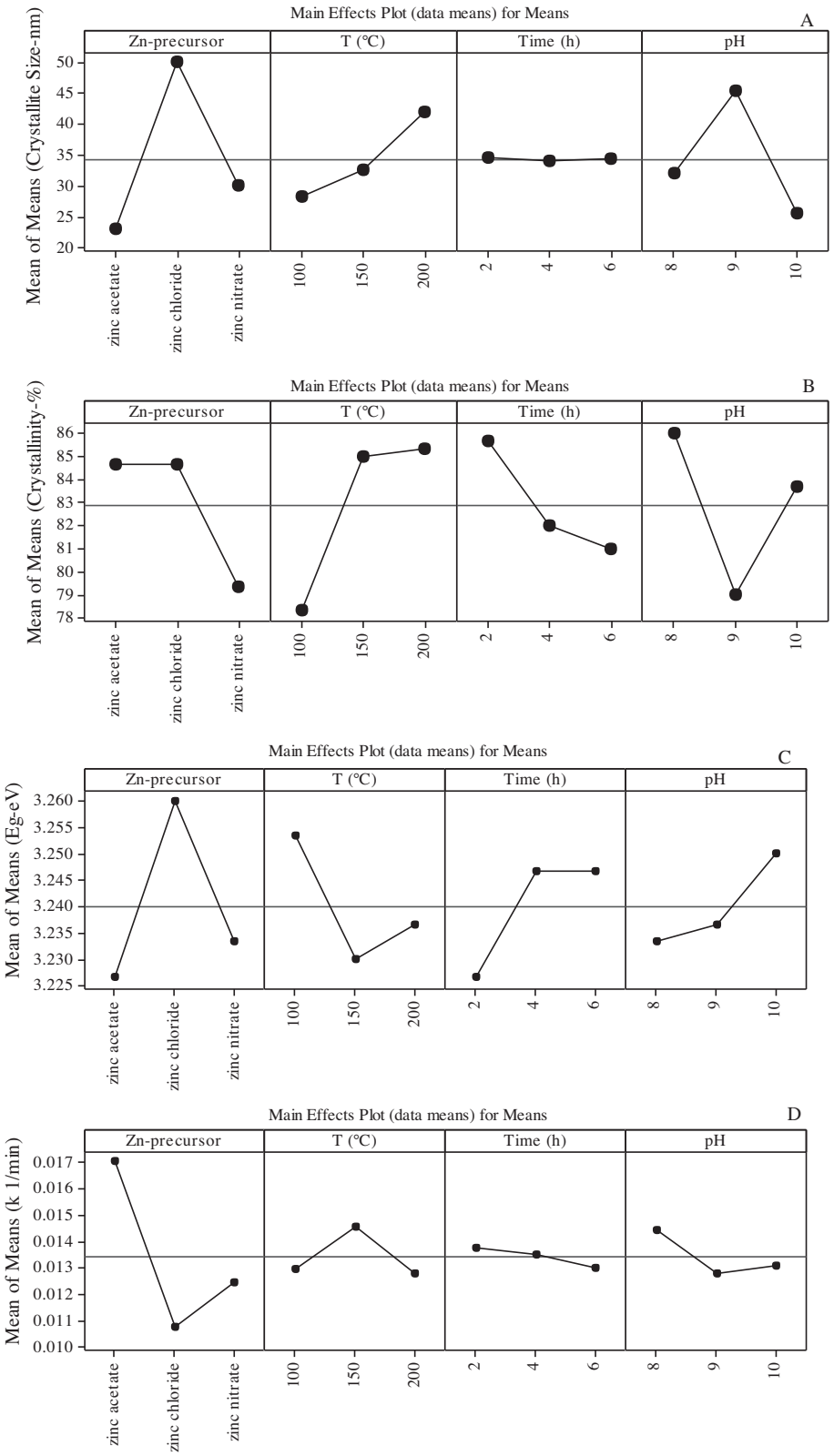

Figure 4. Effects of the design parameters on the crystallite size (A), degree of crystallinity (B), E_g values (C), and k values (D).

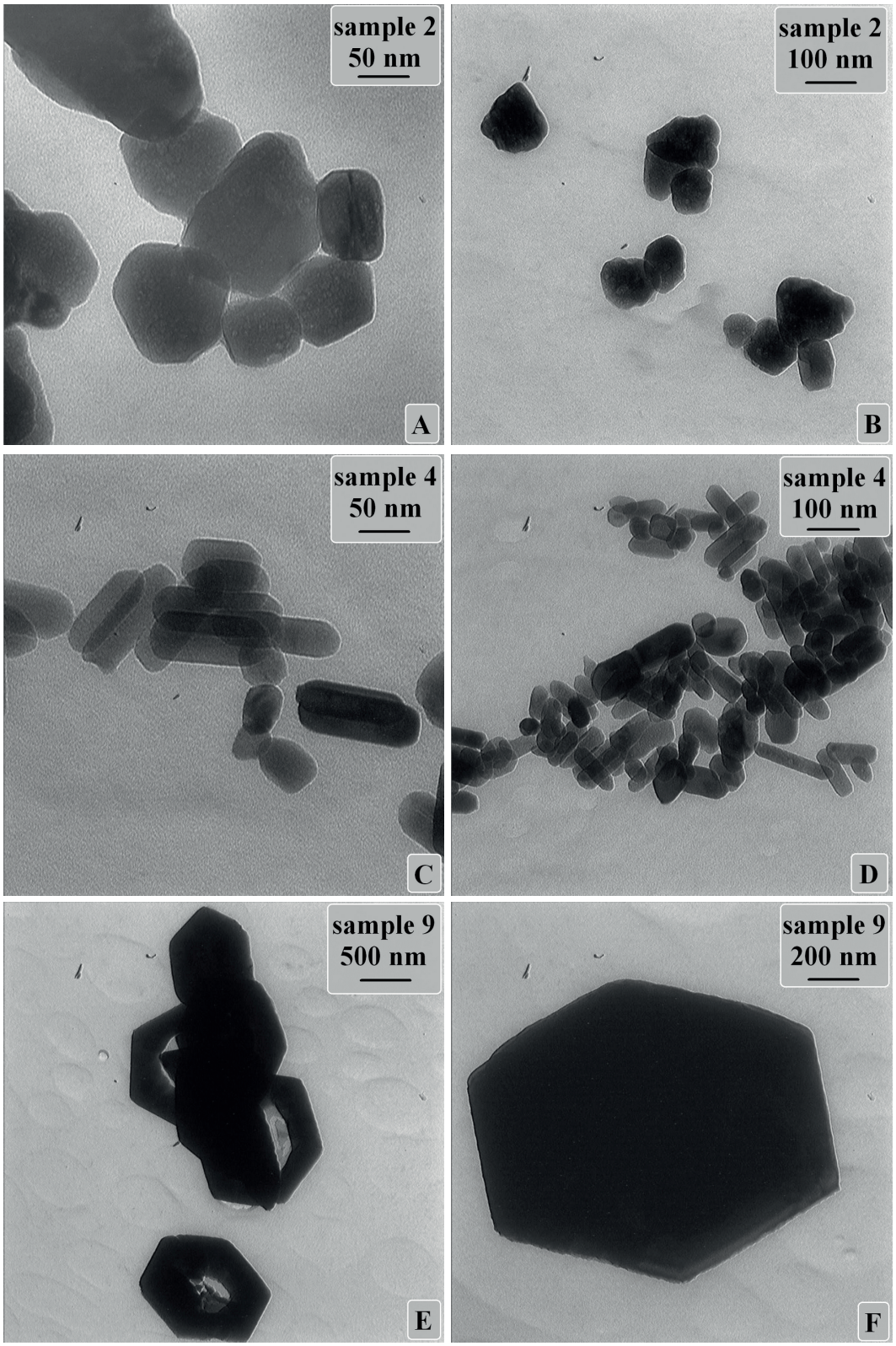

Figure 5. TEM images of the selected samples. A and B) Sample 2, C and D) sample 4, E and F) sample 9.

the crystallite size. When pH is equal to 8, there are several zinc hydroxide complexes in the solution. At the intermediate pH, $Zn(OH)_2$ is the dominant zinc hydroxide complex and leads to formation of bigger particles. By increasing the pH to 10, the condensation process is postponed and leads to the slowing of the particle growth.[44] The third parameter affecting the crystallite size is the hydrothermal temperature. The crystallite size grew with an increase in temperature due to the provision of more energy for nucleation and particle growth. The last parameter is the hydrothermal time, which has no significant effect on the crystallite size.

2.2.2. Degree of crystallinity

Based on Figure 4B and Table 1, pH and temperature are the factors exerting the most influence on the crystallinity. However, it must be mentioned that the effects of the other factors are not negligible. The highest crystallinity is achieved by adjusting the pH to 8. Increasing the pH to 9 significantly decreases crystallinity and more increase in pH (to reach 10) leads to increased crystallinity. This behavior might be attributed to the change in the sol component. ZnO crystallites could be formed and stabilized at elevated pH values,[45] so its higher crystallinity at a pH of 10 might be explained by this phenomenon. Under the lower pH conditions (pH 9), the as-synthesized ZnO crystallites were not stable anymore, and, as a result, particles with lower crystallinity are synthesized.[46] However, particles with the highest crystallinity were formed under the lowest pH value (pH 8), in which more $Zn(OH)_x$ ions as the building units of the ZnO structure exist.[45]

2.2.3. E_g values

Although the difference between E_g values is negligible, the lowest value was achieved by using zinc acetate in a solution with the pH value of 8 and hydrothermal treatment at 150 °C for 2 h. Zn-precursor type is the factor exerting the highest influence on this parameter (see Figure 4C).

2.2.4. k values

This work was conducted to obtain highly active ZnO NPs. To evaluate this, the photocatalytic performances of the as-synthesized powders were measured and reported as k. The highest k value was observed with the sample prepared from zinc acetate precursor in a solution with pH value of 8 and hydrothermal treatment at 150 °C for 2 h (see Figure 4D).

Zinc acetate as the selected Zn-precursor is the factor exerting the highest influence on the crystallite size, E_g values, and consequently k. The lowest crystallite size, the highest crystallinity, and the lowest E_g value were achieved by using this precursor. Each of these factors could have a considerable effect on the photocatalytic behavior, to the effect that if all of them are simultaneously provided, the highest photoactivity will be achieved. The other three parameters, i.e. time, pH, and temperature, have similar impact rates. The selected time was 2 h and Figures 4A–4C show that the highest crystallinity and lowest E_g were obtained under this condition. The average crystallite size was not affected by this parameter. In this way, achievement of the highest k seems to be practical. In relation to the other two parameters (temperature and pH), however, the improvement in k is attributed to the enhanced crystallinity and the decrease of the E_g value.

2.3. Preparation of the optimized samples based on the Taguchi statistical method

The target parameter in this work was k as an index of the photoactivity of the as-synthesized samples. Optimization of the preparation conditions to achieve the highest k value was accomplished using the Taguchi

statistical method. As mentioned before, Zn-precursor type has the greatest effect on k. The impact weights of other factors are relatively similar. Based on the results, it can be predicted that the sample prepared from zinc acetate precursor in a solution with pH of 8 and hydrothermal treatment at 150 °C for 2 h has the highest k value and the highest photocatalytic performance. This sample was prepared and characterized as described below.

Figure 6A shows the XRD pattern of the as-synthesized optimized sample, confirming the formation of ZnO as a unique phase as was observed in the other 9 samples. Based on this result, the crystallinity and crystallite size are calculated as 82% and 15 nm, respectively.

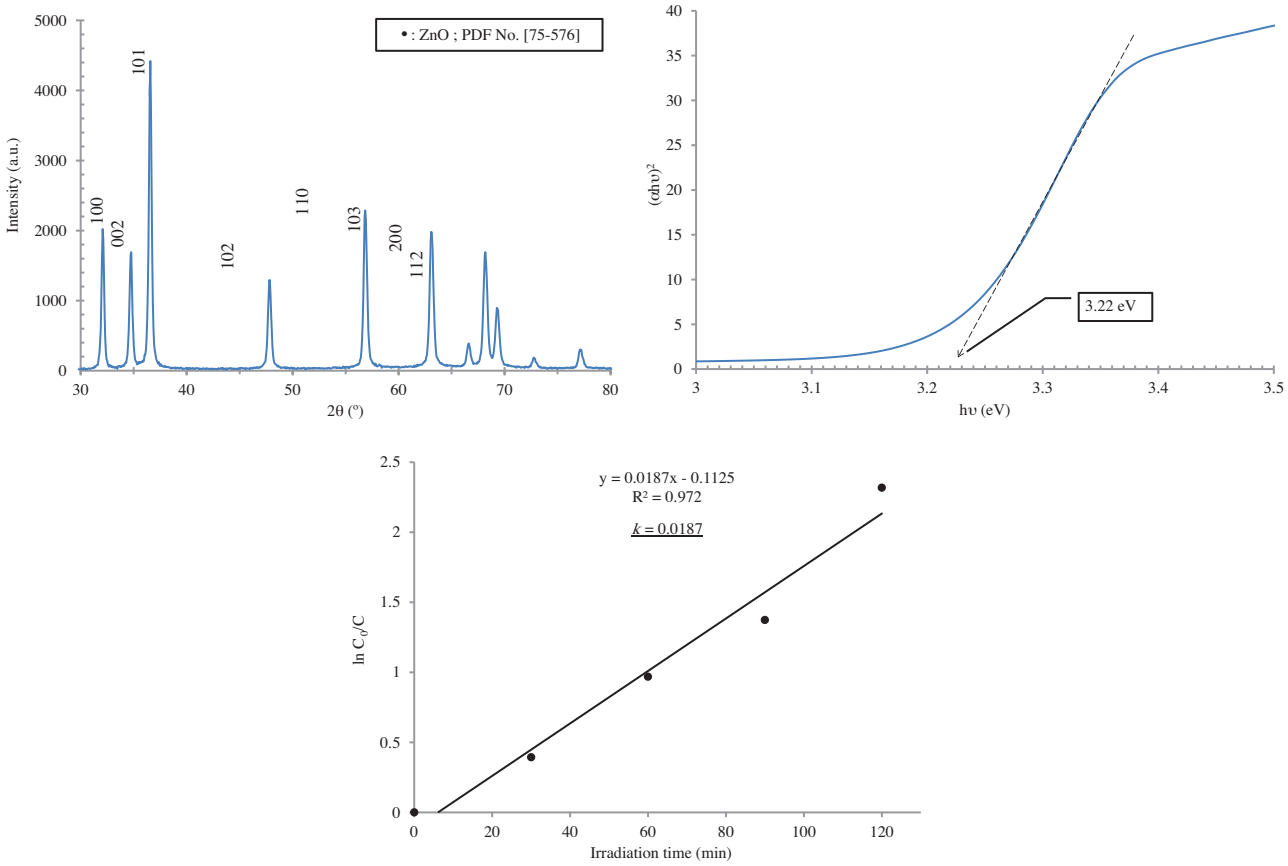

Figure 6. Characteristics of the optimized sample. A) XRD pattern, B) Tauc plot, C) kinetics of the photodegradation of MB solution containing the optimized powder samples.

Figure 6B is related to the DRS results of this sample, showing an E_g value of 3.22 eV, supporting the XRD results. As can be seen, these conditions (i.e. zinc acetate precursor, pH 8, T = 150 °C, and t = 2 h) were relatively effective in increasing the crystallinity and decreasing the crystallite size and E_g value. The influences of these values on photoactivity should be considered. Figure 6C shows the 'ln (C_0/C)' vs. 'UV irradiation time' for the optimized sample. The k value was calculated as 0.0187, which is bigger than those of the other 9 samples. This observation confirmed that the Taguchi method is authentic for optimizing the preparation parameters to achieve the highest photoactivity.

3. Experimental

3.1. Experimental procedure design based on the Taguchi approach

The L9 array of the Taguchi approach was applied to design the experimental plan of this study. For this reason, four variable parameters (Zn-precursor, time and temperature of hydrothermal process, and pH value) were selected and adjusted in three levels. These parameters and their relative values are presented in Table 3. Based on the L9 array of the Taguchi approach, the preparation conditions were defined and are presented in Table 4. The optimization of the mentioned parameters was conducted via the comparison of the means of mean values.

Table 3. Parameters and their relative values for the experimental procedure design.

Factors		Zn-precursor	T (°C)	Time (h)	pH
Levels	1	Zinc nitrate	100	2	8
	2	Zinc acetate	150	4	9
	3	Zinc chloride	200	6	10

3.2. Starting chemicals

The Zn-precursors were zinc nitrate hexahydrate (molecular formula: $Zn(NO_3)_2.6H_2O$, molecular weight = 297.48 g/mol, Merck), zinc acetate dihydrate (chemical formula: $Zn(CH_3COO)_2.2H_2O$, molecular weight = 219.49 g/mol, Merck), and zinc chloride (chemical formula: $ZnCl_2$, molecular weight = 136.30 g/mol, Merck). Triethylamine (TEA, chemical formula: $(C_2H_5)_3N$, molecular weight = 101.19 g/mol, Merck) and distilled water were used as the pH-adjusting agent and solvent, respectively.

3.3. Preparation procedure

Nine samples should be prepared according to the conditions described in Table 4. For this reason, the Zn-precursor and distilled water were mixed and stirred for 1 h to gain a solution with the concentration of 5 g/L. Then TEA was added to the solution under stirring dropwise to adjust the pH to meet the requirements of Table 4. After pH adjustment, the solution was stirred for 1 h and then aged for 24 h at room temperature to gain a white sediment. After that, the solution was hydrothermally treated by an autoclave. The temperature and time of this treatment were adjusted according to Table 4. The instrument was then switched off and cooled down at its natural rate. The obtained suspensions were filtered, washed, and dried at <100 °C to achieve powder samples. A schematic workflow of the synthesis procedure is shown in Figure 7.

3.4. Characterization

The phase component of the as-synthesized samples was determined via XRD analysis, conducted with a PANalytical diffractometer (X'Pert Pro., the Netherlands). The analysis of the XRD patterns was accomplished using PANalytical X'Pert HighScore software. The statistical approaches require numerical data.

To convert the XRD patterns into numerical data, the crystallite sizes and degree of crystallinity of the specimens were calculated. The Williamson–Hall equation ($B.\cos\theta = 0.9\lambda/d + \eta.\sin\theta$) was utilized for estimating the average crystallite size, where d, θ, λ, λ, and B are crystallite size, diffraction angle, wavelength of the X-ray, lattice strain, and the peak full width at half maximum, respectively. Plotting '$B.\cos\theta$' vs. '$\sin\theta$' yields a straight line with the intercept as $0.9\lambda/d$.[47] The crystallinity estimation was made dividing 'sum of

Table 4. Series of the required samples, based on the L9 orthogonal array.

Sample	Factors			
	Zn-precursor	T (°C)	Time (h)	pH
1	Zinc nitrate	100	6	9
2	Zinc nitrate	150	2	10
3	Zinc nitrate	200	4	8
4	Zinc acetate	100	2	8
5	Zinc acetate	150	4	9
6	Zinc acetate	200	6	10
7	Zinc chloride	100	4	10
8	Zinc chloride	150	6	8
9	Zinc chloride	200	2	9

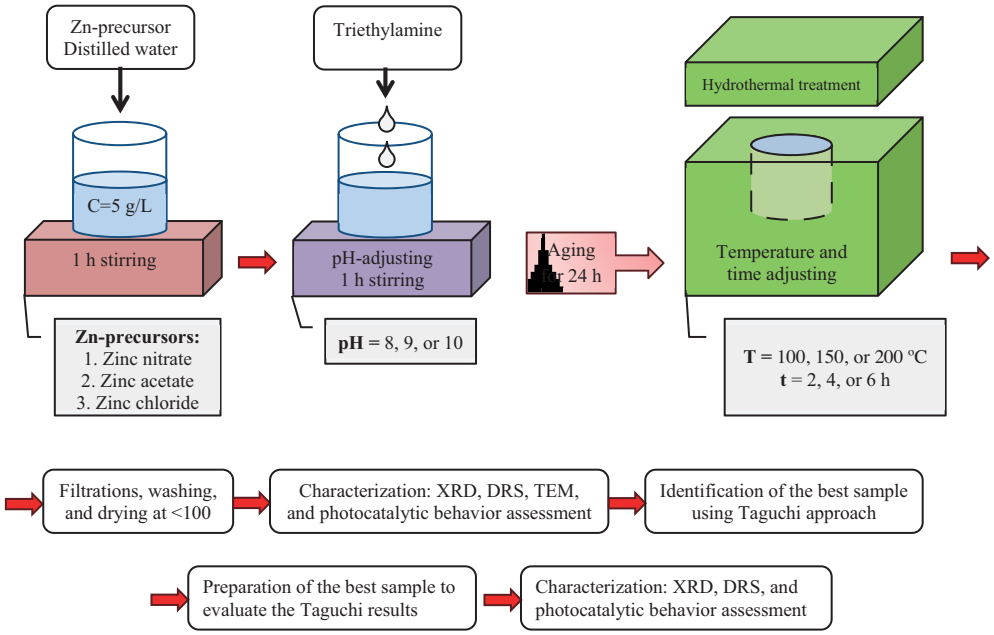

Figure 7. Schematic illustration for the synthesis procedure of ZnO NPs.

net area' by 'sum of total area'. These values were obtained from the PANalytical X'Pert HighScore software. This method has been used previously.[5,31,36,48,49] It should be mentioned that these numerical data are not absolute values but are dependent on many factors and yield relative values to compare the effects of various parameters.

Microscopic images were obtained via transmission electron microscopy (TEM, LEO equipment, Japan). TEM images were utilized to determine particle size of the as-synthesized powder samples.

UV-Vis diffuse reflection spectroscopy (DRS) was carried out with a UV-Vis scanning spectrophotometer (JASCO, Japan). The results of this test were used to determine the direct band gap energy (E_g) via Tauc method, in which '$(\alpha h\upsilon)^2$' was plotted versus '$h\upsilon$', where '$h\upsilon$' and 'α' are the photon energy and the absorption coefficient, respectively. The E_g value is achieved by extrapolating the linear part of the $(\alpha h\upsilon)^2$ vs. $h\upsilon$ plot

to its intersection with the hυ-axis.[31,50]

The photoactivity of the samples was measured by evaluating the degradation of methylene blue (MB) under UV irradiation. The MB solution was prepared with a concentration of 30 mg/L. Powder samples (100 mg) were mixed with 100 mL of MB solution and used for photodegradation measurements. Two UV lamps with a power of 15 W and a wavelength of 365 nm were utilized to irradiate the solutions. Then the solid part was separated from the irradiated MB solution and the changes of MB concentration were measured. The decomposition rate of MB vs. irradiation time (k) was obtained from the $\ln(C_0/C)$ vs. irradiation time curve (C_0 and C values are MB concentration without irradiation and after irradiation, respectively).

References

1. Hasnidawani, J. N.; Azlina, H. N.; Norita, H.; Bonnia, N. N.; Ratim, S.; Ali, E. S. *Procedia Chem.* **2016**, *19*, 211-216.
2. Genç, A. *Ceram. Int.* **2017**, *43*, 1710-1715.
3. Urgessa, Z. N.; Botha, J. R.; Tankio Djiokap, S. R.; Coleman, C.; Bhattacharyya, S. *Physica B* (in press).
4. Li, M.; Liu, X. L.; Cui, D. L.; Xu, H. Y.; Jiang, M. H. *Mater. Res. Bull.* **2006**, *41*, 1259-1265.
5. Gharagozlou, M.; Naghibi, S. *J. Chin. Chem. Soc.-Taip.* **2016**, *63*, 290-297.
6. El-Shazly, A. N.; Rashad, M. M.; Abdel-Aal, E. A.; Ibrahim, I. A.; El-Shahat, M. F.; Shalan, A. E. *J. Environ. Chem. Eng.* **2016**, *4*, 3177-3184.
7. Li, W.; Xu, H.; Yu, H.; Zhai, T.; Xu, Q.; Yang, X.; Wang, J.; Cao, B. *J. Alloy. Compd.* **2017**, *706*, 461-469.
8. Lim, J. W.; Hwang, D. K.; Lim, K. Y.; Kang, M.; Shin, S. C.; Kim, H. S.; Choi, W. K.; Shim, J. W. *Sol. Energ. Mat. Sol. C.* **2017**, *169*, 28-32.
9. Khaghanpour, Z.; Naghibi, S. *J. Nanostruct. Chem.* **2017**, *7*, 55-59.
10. Di Mauro, A.; Fragalà, M. E.; Privitera, V.; Impellizzeri, G. *Mat. Sci. Semicon. Proc.* **2017**, *69*, 44-51.
11. Luo, Q.; Xu, P.; Qiu, Y.; Cheng, Z.; Chang, X.; Fan, H. *Mater. Lett.* **2017**, *198*, 192-195.
12. Deshmukh, P. R.; Sohn, Y.; Shin, W. G. *J. Alloy. Compd.* **2017**, *711*, 573-580.
13. Gupta, V. K.; Sadeghi, R.; Karimi, F. *Sensor. Actuat. B-Chem.* **2013**, *186*, 603-609.
14. Gharagozlou, M.; Naghibi, S. *Mater. Res. Bull.* **2016**, *84*, 71-78.
15. Guan, W.; Zhang, L.; Wang, C.; Wang, Y. *Mat. Sci. Semicon. Proc.* **2017**, *66*, 247-252.
16. Murugadoss, G. *J. Mater. Sci. Technol.* **2012**, *28*, 587-593.
17. Kang, W.; Jimeng, X.; Xitao, W. *Appl. Surf. Sci.* **2016**, *360*, 270-275.
18. Cao, M.; Wang, F.; Zhu, J.; Zhang, X.; Qin, Y.; Wang, L. *Mater. Lett.* **2017**, *192*, 1-4.
19. Samadipakchin, P.; Mortaheb, H. R.; Zolfaghari, A. *J. Photoch. Photobio. A* **2017**, *337*, 91-99.
20. Hatamvand, M.; Mirjalili, S. A.; Sharzehee, M.; Behjat, A.; Jabbari, M.; Skrifvars, M. *Optik* **2017**, *140*, 443-450.
21. De Marco, L.; Calestani, D.; Qualtieri, A.; Giannuzzi, R.; Manca, M.; Ferro, P.; Gigli, G.; Listorti, A.; Mosca, R. *Sol. Energ. Mat. Sol. C.* **2017**, *168*, 227-233.
22. Fragalà, M. E.; Di Mauro, A.; Cristaldi, D. A.; Cantarella, M.; Impellizzeri, G.; Privitera, V. *J. Photoch. Photobio. A* **2017**, *332*, 497-504.
23. Bora, T.; Sathe, P.; Laxman, K.; Dobretsov, S.; Dutta, J. *Catal. Today* **2017**, *284*, 11-18.
24. Gu, B.; Pliss, A.; Kuzmin, A. N.; Baev, A.; Ohulchanskyy, T. Y.; Damasco, J. A.; Yong, K. T.; Wen, S.; Prasad, P. N. *Biomaterials* **2016**, *104*, 78-86.

25. Hariharan, R.; Senthilkumar, S.; Suganthi, A.; Rajarajan, M. *J. Photoch. Photobio. B* **2012**, *116*, 56-65.
26. Senthilkumar, S.; Hariharan, R.; Suganthi, A.; Ashokkumar, M.; Rajarajan, M.; Pitchumani, K. *Powder Technol.* **2013**, *237*, 497-505.
27. Ashraf, R.; Riaz, S.; Hussain, S. S.; Naseem, S. *Mater. Today-Proc.* **2015**, *2*, 5754-5759.
28. Xian, F.; Zheng, G.; Xu, L.; Kuang, W.; Pei, S.; Cao, Z.; Li, J.; Lai, M. *J. Alloy. Compd.* **2017**, *710*, 695-701.
29. Kim, Y.; Kang, S. *Acta Mater.* **2011**, *59*, 3024-3031.
30. Özdal, T.; Taktakoğlu, R.; Özdamar, H.; Esen, M.; Takçı, D. K.; Kavak, H. *Thin Solid Films* **2015**, *592*, 143-149.
31. Naghibi, S.; Faghihi Sani, M. A.; Madaah Hosseini, H. R. *Ceram. Int.* **2014**, *40*, 4193-4201.
32. Hassanpour, A.; Bogdan, N.; Capobianco, J. A.; Bianucci, P. *Mater. Design* **2017**, *119*, 464-469.
33. Kumaresan, N.; Ramamurthi, K.; Ramesh Babu, R.; Sethuraman, K.; Moorthy Babu, S. *Appl. Surf. Sci.* **2017**, *418A*, 138-146.
34. Empizo, M. J. F.; Santos-Putungan, A. B.; Yamanoi, K.; Salazar, H. T. Jr.; Anguluan, E. P.; Mori, K.; Arita, R.; Minami, Y.; Luong, M. V.; Shimizu, T. et al. *Opt. Mater.* **2017**, *65*, 82-87.
35. Naghibi, S.; Jamshidi, A.; Torabi, O.; Kahrizsangi, R. E. *Int. J. Appl. Ceram. Tec.* **2014**, *11*, 901-910.
36. Jamshidi, A.; Nourbakhsh, A. A.; Naghibi, S.; Mackenzie, K. J. D. *Ceram. Int.* **2014**, *40*, 263-271.
37. Chung, Y. T.; Ba-Abbad, M. M.; Mohammad, A. W.; Hairom, N. H. H.; Benamor, A. *Mater. Design* **2015**, *87*, 780-787.
38. Kim, K. D.; Choi, D. W.; Choa, Y. H.; Kim, H. T. *Colloid. Surface. A* **2007**, *311*, 170-173.
39. Ohira, T.; Yamamoto, O. *Chem. Eng. Sci.* **2012**, *68*, 355-361.
40. Pourrahimi, A. M.; Liu, D.; Pallon, L. K. H.; Andersson, R. L.; Martinez Abad, A.; Lagaron, J. M.; Hedenqvist, M. S.; Strom, V.; Gedde, U. W.; Olsson, R. T. *RSC Adv.* **2014**, *4*, 35568-35577.
41. Ahsanulhaq, Q.; Umar, A.; Hahn, Y. B. *Nanotechnology* **2007**, *18*, 115603.
42. Wilson, H. F.; Tang, C.; Barnard, A. S. *J. Phys. Chem. C.* **2016**, *120*, 9498-9505.
43. Xu, L.; Hu, Y. L.; Pelligra, C.; Chen, C. H.; Jin, L.; Huang, H.; Sithambaram, S.; Aindow, M.; Joesten, R.; Suib, S. L. *Chem. Mater.* **2009**, *21*, 2875-2885.
44. Alias, S. S.; Ismail, A. B.; Mohamad, A. A. *J. Alloy. Compd.* **2010**, *499*, 231-237.
45. Søndergaard, M.; Bøjesen, E. D.; Christensen, M.; Iversen, B. B. *Cryst. Growth Des.* **2011**, *11*, 4027-4033.
46. McBride, R. A.; Kelly, J. M.; Mccormack, D. E. *J. Mater. Chem.* **2003**, *13*, 1196-1201.
47. Williamson, G. K.; Hall, W. H. *Acta Metall. Mater.* **1953**, *1*, 22-31.
48. Torabi, O.; Naghibi, S.; Golabgir, M. H.; Jamshidi, A. *J. Chin. Chem. Soc.-Taip.* **2016**, *63*, 379-384.
49. Naghibi, S.; Sheikhi, E. *J. Adv. Mater. Proc.* **2016**, *4*, 46-55.
50. Viezbicke, B. D.; Patel, S.; Davis, B. E.; Birnie, D. P. *Phys. Status Solidi B* **2015**, *252*, 1700-1710.